AIAA JOURNAL
Vol. 36, No. 6, June 1998

Some Specific Characteristics of Turbulence in the Reactive Wakes of Bluff Bodies

Stéphane Sanquer,* Pascal Bruel,† and Bruno Deshaies‡
Centre National de la Recherche Scientifique, Futuroscope 86960, France

The results of a detailed experimental analysis of the flows associated with bluff-body stabilized premixed combustion are presented. The experimental setup has been designed to facilitate as much as possible the test of numerical predictions of such a flow geometry. The boundary conditions are well defined and easy to reproduce from a numerical point of view. The results reported here are based principally on velocity measurements using a four-beam two-color laser Doppler velocimeter. As far as the mean structure of the wakes is concerned and confirming in that respect the results reported in the literature, it is shown that the presence of combustion leads only to quantitative changes of the mean structure of the reactive wakes when compared with their inert counterparts. This is no longer the case when the statistical and spectral properties of the wakes are considered. Indeed, a complete restructuring of the instantaneous flow structure induced by dramatic changes of the large-scale motion properties is observed when combustion is developing in the wake. The reacting wakes are characterized by the absence of the vortex shedding observed in inert wakes, but depending on the equivalence ratio of the incoming mixture, a longitudinal pulsation associated with the symmetric flapping of the flame fronts anchored at the flame holder edges can be observed.

I. Introduction

TURBULENT reactive wakes that develop in premixed reacting flows behind a bluff body are known to feature multiscale unsteadiness. As far as inert wakes are concerned, numerous experimental,[1–3] and numerical studies[4,5] show that this multiscale unsteadiness is the result of the interaction between large-scale coherent structures, i.e., the vortices shedded alternatively from the bluff-body edges and small-scale turbulence. Thus, the distribution of the energy contained in the flow can be expected to be modified in presence of combustion in the wake. The first evidence of this change is given by Williams et al.,[6] who essentially use strioscopic visualizations of the flow and pressure measurements. As a tentative explanation, these authors suggest that the vortex shedding disappears in the presence of combustion in the wake of the obstacle.

Since the work of Williams et al.,[6] most of the experimental studies reported in the literature are related to the characterization of the structure of the mean flow.[7–9] The first experimental study that gives some insight into the change of the unsteady structure of wakes behind bluff bodies with and without combustion is due to Fujii and Eguchi,[10] who take advantage of the laser Doppler anemometry to show a dramatic reduction of the turbulent kinetic energy level between inert and combusting flows. Following Williams et al.,[6] Fujii and Eguchi[10] attribute such a reduction to the absence of vortex shedding in the reacting wakes.

As far as the modeling of such a type of flow is concerned, the fact that the mean flow is not always the most probable calls for the use of specific modeling approaches to predict, for instance, the level of production of pollutants whose mechanisms of formation are known to depend on the unsteady properties of the flow. Among the various modeling strategies, the large-eddy simulation[11] (LES) appears to be one of the most attractive. Indeed, by simulating the large-scale structures while modeling through a subgrid scale (SGS) model the smaller ones, supposed to be more isotropic, the LES approach represents a good compromise between the direct numerical simulation, which is still limited to low-Reynolds-number flows, and the conventional modeling based on the closure of the averaged Navier–Stokes equations.

Evaluation of the performances of LES requires the availability of experimental data obtained on flow geometries that provide most of the prominent phenomena of practical interest (large-scale structures and flame–wall interaction) and for which the boundary conditions are well defined and easily reproducible from a numerical point of view. In that framework, the geometry investigated by Williams et al.[6] and Fujii and Eguchi[10] appears to be a good candidate to meet these requirements. Indeed, such a flow geometry is simple and features large-scale structures as well as flame–wall interaction. Moreover, the development of the incoming flow is not influenced by the obstacle holding system, allowing the obtaining of well-defined incoming flow characteristics upstream of the flame holder.

As far as the evaluation of the predictive capabilities of LES on such a geometry is concerned, the mean flow properties (velocity and species concentrations or temperature profiles) have been the main subject of comparison presented in the numerical studies reported in the literature, whereas only a limited number of comparisons performed in terms of probability density functions (PDFs) are presented.[12,13]

The constant evolution[14] and the need for improvement of SGS models call for comparison with experimental results that include more systematically the unsteady flow properties presented in a form directly exploitable for an LES test (PDFs and spectra). Thus the purpose of the present experimental study is to provide, mainly through velocity measurements, a comparison between inert and reacting wakes of bluff bodies in terms of their unsteady properties that includes, in particular, velocity PDFs as well as the related spectra.

II. Experimental Setup

Figure 1 shows a schematic diagram of the experimental setup. The shape of the three steel flame stabilizers used for these experiments and the corresponding spatial coordinate system are given in Fig. 2. The abscissa $x = 0$ corresponds to the rear face of the obstacles, $y = 0$ corresponds to the horizontal plane of symmetry located at one-half of the channel height, and the vertical plane $z = 0$ is located at one-half of the channel width. The geometry has been chosen to provide a two-dimensional mean flow at the entrance of the test section, and the flow characteristics are, a priori, as close

Presented as Paper 96-3034 at the AIAA/ASME/SAE/ASEE 32nd Joint Propulsion Conference, Lake Buena Vista, FL, July 1–3, 1996; received Feb. 6, 1997; revision received Dec. 11, 1997; accepted for publication Jan. 7, 1998.

*Doctorant, Laboratoire de Combustion et de Détonique, Ecole Nationale Supérieure de Mécanique et d'Aérotechnique, B.P. 109.

†Chargé de Recherche, Laboratoire de Combustion et de Détonique, Ecole Nationale Supérieure de Mécanique et d'Aérotechnique, B.P. 109.

‡Directeur de Recherche, Laboratoire de Combustion et de Détonique, Ecole Nationale Supérieure de Mécanique et d'Aérotechnique, B.P. 109. E-mail: deshaies@lcd.univ-poitiers.fr.

Table 1 Main parameters of the wakes (maximum random error in $U_{axis} = \pm 0.01$ m/s, maximum relative uncertainty in $U_\tau = \pm 8\%$, and maximum relative uncertainty in $X_r = \pm 7\%$)

Case	Shape of the cross section of the obstacle	B, %	Φ	Flow rate, 1/s	U_{axis}, m/s	U_τ, m/s	Re_{ch}	Re_{obs}	T_{obs}, K	X_r, mm
i1	Triangular	33	Inert	12	3.1	0.15	6.684×10^3	2.228×10^3	——	19
i2	Triangular	50	Inert	24	5.3	0.25	11.581×10^3	5.790×10^3	——	42
i3	Triangular	33	Inert	36	8.1	0.37	17.484×10^3	5.828×10^3	——	15
i4	Rectangular	33	Inert	36	7.9	0.39	17.052×10^3	5.684×10^3	——	10
r1	Triangular	33	0.65	12	2.9	0.11	6.253×10^3	2.084×10^3	513	23
r2	Triangular	50	0.65	24	5.1	0.24	11.114×10^3	5.572×10^3	513	51
r3	Triangular	33	0.65	36	7.6	0.38	16.404×10^3	5.468×10^3	513	40
r4	Rectangular	33	0.65	36	7.6	0.38	16.404×10^3	5.468×10^3	698	40
r5	Triangular	33	0.85	36	7.5	0.40	16.189×10^3	5.396×10^3	773	19

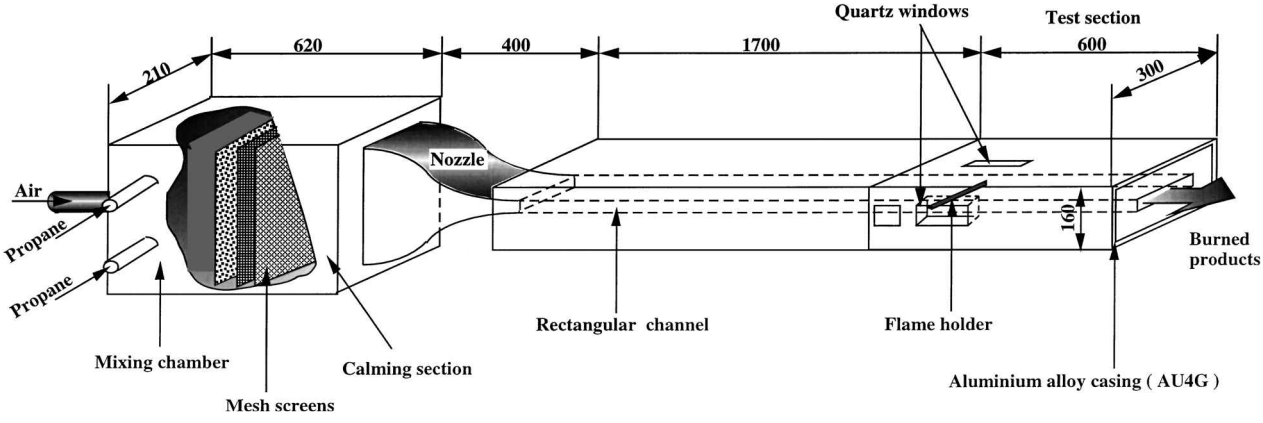

Fig. 1 Schematic of the test facility (all dimensions in millimeters).

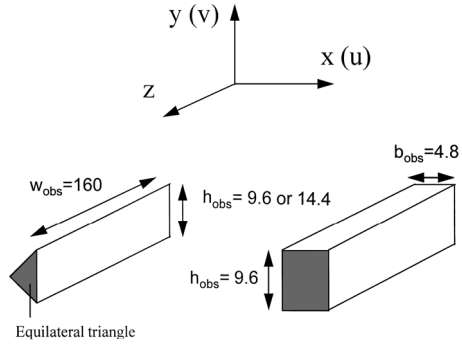

Fig. 2 Shape and dimensions of the flame holders (all dimensions in millimeters).

as possible to those of a fully developed turbulent channel flow. The test section consists essentially of a 2.30-m-long channel of a 160×28.8 mm rectangular constant cross section made of an arrangement of 55-mm-thick refractory bricks maintained together by an aluminum alloy casing. The side walls of the channel incorporate quartz windows for optical access. An obstacle that spans from side wall to side wall is mounted symmetrically at a distance of 1.86 m from the channel entrance. The fuel (commercial propane) and the air supplied to the test rig from high-pressure storage tanks are premixed in a mixing chamber that is followed by a settling chamber that homogenizes the mixture. The temperature of the flow at the entrance of the test section is 280 ± 5 K. A chromatographic analysis of the fuel reveals the following composition (in volume): 1.66% C_2H_6, 84.66% C_3H_8, 12.30% C_3H_6, and 1.38% C_4H_{10}, leading to the global formula $C_{2.997}H_{7.748}$.

The incoming flow is characterized by its equivalence ratio ϕ and its Reynolds number Re_{ch}. The equivalence ϕ of the incoming flow is based on the global definition of the fuel. To reveal the influence of this parameter on the time evolution of the flowfield, two different values are considered, namely, $\phi = 0.65$ and $\phi = 0.85$, that correspond to an adiabatic flame temperature at ambient pressure of 1753 and 2080 K, respectively. Because of the long duration of the experiment, the incoming flow equivalence ratio is continuously controlled by a Leybold–Heraeus propane analyzer. Thus the relative variation of ϕ is within $\pm 3.0\%$ of the nominal desired value. The Reynolds number Re_{ch} is based on the channel height h_{ch}, i.e., $Re_{ch} = (U_{axis} \times h_{ch})/\nu_0$, where ν_0 stands for the kinematic viscosity of the incoming mixture. U_{axis} is the mean velocity measured upstream of the flame holder on the channel centerline ($y = 0$, $z = 0$) at the abscissa $x = -160$ mm. The obstacle is characterized by its size and shape (Fig. 2) defined by $B = Re_{obs}/Re_{ch}$, where $Re_{obs} = (U_{axis} \times h_{obs})/\nu_0$; h_{obs} is the flame holder height.

Table 1 lists the main characteristics associated with the incoming flow properties of the nine cases studied. Cases i1–i4 correspond to the isothermal wakes, whereas cases r1–r5 correspond to the reacting wakes.

III. Measurement Equipment and Data Processing

A four-beam two-color laser Doppler velocimeter (LDV) system is used for the velocity measurements. The beams are frequency shifted by Bragg cells to avoid any directional ambiguity. The principal characteristics of the system are listed in Table 2. In all cases, the flow is seeded with submicron-sized SiO_2 and TiO_2 particles. The two velocity components (u for the axial x direction and v for the normal y direction) are measured in the forward-scattering mode to maximize the signal-to-noise ratio. The scattered signal is collected by two photomultipliers, processed by two Dantec 57N10 burst spectrum analysers (BSA) and sent through an Institute of Electrical and Electronics Engineers (IEEE) 488 interface to a microcomputer for storage and postprocessing. The same microcomputer controls in real time through a serial line the Charly robot system that displaces the LDV probe and the collecting optics.

The probe volume has a length of approximately 4 mm and a diameter of 0.2 mm. The depth of field of the photomultiplier is 0.5 mm. The minimum step of displacement of the probe volume is equal to 0.1 mm in the three directions. The exact position of the effective measuring volume inside of the probe volume remains unknown, but relative positions are known with an accuracy of ± 0.01 mm.

The fast Fourier transform for each validated burst, i.e., a burst for which the ratio between the global maximum and the two largest

Table 2 Characteristics of the two-component LDV system

Characteristic	Laser beam color	
	Green	Blue
4-W argon laser wavelength, nm	514.5	488
Input lens focal length, mm	400	400
Beams intersection half-angle, deg	2.87	2.87
Photomultiplier lens focal length, mm	700	700
Fringe spacing, μm	5.14	4.88
Laser beam e^{-2} size, mm	1.25	1.22
LDV spot diameter, mm	0.21	0.204
LDV spot length, mm	4.2	4.08

local maxima is greater than 4, is performed using 32 samples of the input signal. At each point of measurements, the center frequency and the span around it are chosen to maximize the percentage of burst validation. The maximum validated data rate is 3 kHz for cold flows and 1.5 kHz for reacting flows. The exploration of the flow is performed automatically on a predefined two-dimensional mesh of typically 200–1000 grid points. For each velocity component, five blocks of 2000 measurements each (particle arrival time, particle transit time, and instantaneous velocity) are collected simultaneously. Velocity fluctuations spectra are obtained by evenly sampling the BSA digital signal outputs with the sample and hold technique.[15] The frequency of the sampling is chosen to be twice the mean frequency of the sampled signal. Then, a fast Fourier transform is performed on 5 sets of 1024 samples to obtain the power spectral density (PSD) at each measurement point.

With the present system, the most important source of systematic error is due to the uncertainty associated with the measuring volume positioning relative to the setup axis and the velocity bias. The principal source of random errors affecting the accuracy of the measurements is associated with the statistical uncertainty of the signal sampling.

Taking into account the geometrical characteristics of the effective measuring volume and of the displacement system, the error in determining the location of the measuring volume is estimated to be equal to ± 0.5 mm in the three directions. The statistical bias of the final measured velocity towards higher values is corrected by the sample and hold technique.[16] This procedure is implemented here by using the interarrival time as the weighting factor. This interarrival time is calculated from the particle arrival and transit time data.

Concerning the random errors, a recent paper by Benedict and Gould[17] presents the state of the art in the evaluation of uncertainty estimates for turbulence statistics. For instance, these authors give formulas that can be used to estimate a confidence interval for the rth-order central moment sampling statistic of a random variable P regardless of the underlying distribution of P. Such a generalization represents a breakthrough in uncertainty estimates because so far, as pointed out by Benedict and Gould,[17] the formulas widely used to determine the usual confidence intervals were obtained by supposing that the random variable P was normally distributed. Whatever the strategy adopted, a necessary requirement for any confidence interval determination is the fact that the process under study has to be random. In the present flow configuration, the velocity signal can be considered as random in all considered cases only upstream of the flame holder. Indeed, in the inert wakes, the presence of vortex shedding makes the velocity signal deviate strongly from purely random behavior, as is also the case for two reacting wakes. Accordingly, the random errors associated with the present velocity measurements are evaluated as follows: for the measurements performed upstream of the obstacles, a 95% confidence interval is determined by using the Benedict and Gould[17] formulas. For the measurements performed in the wakes, the average obtained from the 10,000 samples is considered to be the accurate one, and the random errors are estimated from the standard deviation around this accurate value of the averages calculated on blocks of 2000 samples. This latter procedure is also used to evaluate the random estimate associated with the PDFs and the spectra.

The mean surface temperature of the obstacle, needed in particular to correctly describe the boundary conditions for any related numerical computations, is measured using acrylic thermal paints (thermographics), and the results are given in Table 1. The accuracy of these measurements is ± 30 K.

Two examples of temperature spectra are presented in the last part of the results section. For a similar geometry, mean temperature and rms fluctuations, as well as some examples of temperature PDFs obtained by coherent anti-Stokes Raman spectroscopy (CARS), can be found in the study of Fureby and Möller.[13] The present temperature measurements have been obtained by using fine-wire uncoated 20-μm Pt/Pt-10%Rh thermocouples. These homemade thermocouples are built up in such a way that the junction diameter is equal to the wire diameter with an estimated uncertainty of $\pm 20\%$. The analog thermocouple emf signal is amplified and filtered. A one-stage amplifier is used, and the total gain is 320 V/V. The filter has a 3-dB bandwidth of 2.2 kHz with a rolloff of 20 dB/decade. The noise level is below 10 mV, which corresponds to 0.1% of the full-scale deflection, and results in a temperature uncertainty of ± 2 K. The analog signal is sampled at a frequency of 5 kHz through a 12-bit analog-to-digital converter, and the corresponding resolution is less than 1 K. At each point, five sets of 1024 temperature values are stored. The thermal inertia is numerically compensated. The Collis and Williams[18] relation with a Moffat correction[19] is used. For thermocouples for which the geometry junction is sufficiently close to the wire diameter, this procedure provides a reasonable estimation of the time constant as shown by Heitor et al.[20] The Reynolds number used to calculate the time constant is obtained by using the LDV measured value of the mean velocity modulus at the point where the temperature is measured. Radiation losses and catalytic effects that are known to play a significant role in determining the level of the mean temperature and of its rms fluctuations[21] are expected to play a minor role in the characteristics of the temperature spectra that are of interest in the present study, i.e., the peaks of energy in the spectrum. Indeed, the radiative exchanges are made principally with the walls, which are made of a thick refractory material. Accordingly, the wall temperature is varying slowly, and consequently, the radiative exchanges cannot be the cause of the frequency peaks that are observed in some cases of reacting wakes. Finally, the catalytic effect is not known to lead to an oscillatory behavior of the temperature with a specific signature on the temperature spectrum. The mean spectra that are presented correspond to the average of the five calculated spectra. The dispersion of the five spectra around the mean spectrum is used as an estimate of the random error.

IV. Results

Incoming Flow Properties

In all cases, the flow upstream of the bluff bodies presents all the characteristics of a fully developed turbulent channel flow whose mean velocity profiles are nearly two dimensional in the spanwise direction z. Indeed, a variation of only $\pm 2\%$ of the mean streamwise velocity is observed in the spanwise direction over roughly two-thirds of the channel width.

Mean velocity profiles are plotted in Fig. 3, and the corresponding rms velocity fluctuations are given in Fig. 4. The agreement with the results obtained by Comte-Bellot[22] and Eckelmann[23] is good except for cases r1 and r5 for which larger levels of fluctuations are observed. For these two cases, the combustion process developing in the wake is influencing the flow upstream of the flame holder, this effect being more pronounced for the longitudinal stress in cases r1 and r5. This can be related to the pulsating behavior of the reactive wake observed in these two cases. Nevertheless, in all cases, the flow upstream of the bluff body presents at $x = -160$ mm all the overall characteristics of a fully developed flow. Indeed, for x varying between -130 and -160 mm, the mean velocity and the rms fluctuations prove to vary by less than 1%.

To facilitate the computations of the present flow, Table 1 gives the values of the skin-friction velocity $U_\tau = [\nu_0(\partial\langle U\rangle/\partial y)]^{1/2}|_{\text{wall}}$, which have been calculated by using the logarithmic behavior of the mean streamwise velocity component profiles.

Mean Properties of the Wakes

Because this study is mainly devoted to the description of the unsteady behavior of the wakes, only the main mean properties of the wakes that confirm and complement the ones already given

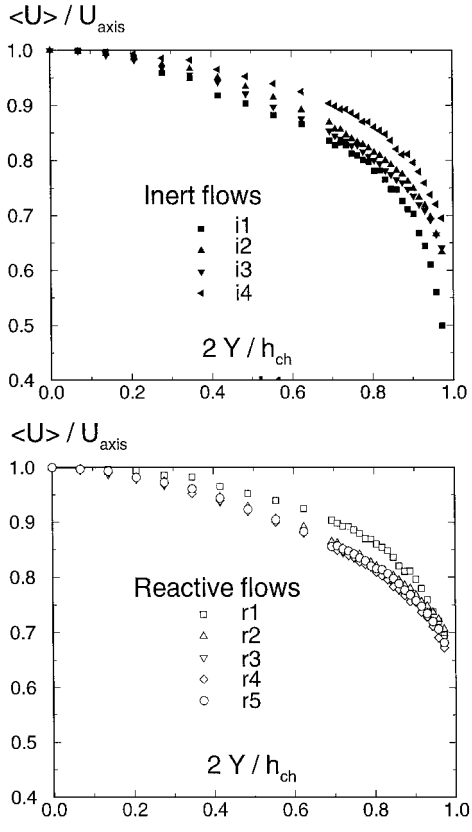

Fig. 3 Transverse profiles of the inlet mean streamwise velocity component at 160 ± 0.5 mm upstream of the flame holder (systematic error in $2y/h_{ch} = \pm 0.035$; random error in U_{axis}, see Table 1; maximum random error in $\langle U \rangle = \pm 0.035$ m/s).

in the literature[6,10] are presented here. An important characteristic of the wakes is the length X_r of the mean recirculation zone, which is known to depend on the Reynolds numbers Re_{ch} and Re_{obs}, the blockage ratio B, the equivalence ratio ϕ, and the obstacle shape. The measured values of X_r, given in Table 1, confirm the following points.

1) For given values of Re_{ch} and Re_{obs}, X_r is always larger in the reactive wakes than it is in the inert wakes.

2) For a given value of B, X_r is an increasing (respectively decreasing) function of Re_{ch} for the reactive (respectively inert) wakes.

3) For the reactive (respectively inert) wakes, X_r is obstacle shape independent (respectively dependent).

4) For the reactive wakes of lean mixtures ($\phi < 1$), X_r is a decreasing function of ϕ.

Now, the following question can be raised: do the wakes exhibit any kind of similarity of their mean structure? To answer that question, one first has to rescale the wakes in the streamwise direction x. To do so, the centerline evolution of the normalized mean longitudinal velocity component, i.e., $\langle U \rangle / U_{axis}$, is plotted against the normalized abscissa x/X_r. Thus, as shown in Fig. 5, three regions are put into evidence: Region 1 is the mean recirculation zone ($x/X_r \leq 1$), region 2 is the near wake ($1 < x/X_r \leq 2$), and region 3 is the far wake ($2 < x/X_r$). Due to the large values of X_r observed in cases i1, r2, r3, and r4, no measurement points belong to region 3 for these cases. Accordingly, we shall concentrate our analysis mainly on regions 1 and 2.

The rescaling in the y direction is done by using half of the height of the channel as the reference length scale. Thus, at the end of region 1 ($x/X_r = 1$) and within region 2 ($x/X_r = 1.4$) the transverse profiles of the normalized mean velocity components are plotted in Fig. 6 against the normalized transverse coordinate. The analysis of Figs. 5 and 6 reveals the following.

1) For inert wakes, the rescaling used here is fair for obstacles of the same shape (triangular section) but do not rescale the sensitivity of the wakes to the obstacle shape. Moreover, the rescaled profiles

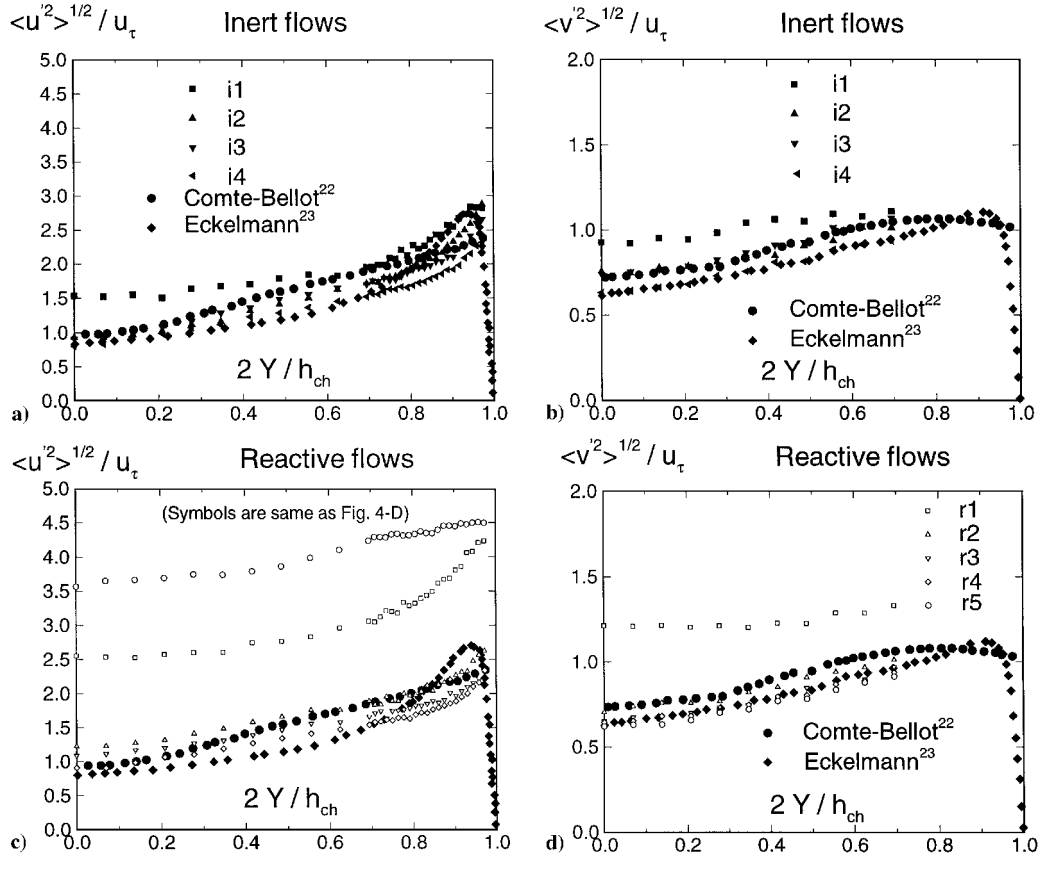

Fig. 4 Transverse profiles of the turbulence velocity data at 160 ± 0.5 mm upstream of the flame holder: a) and b) inert flows and c) and d) reacting flows (systematic error in $2y/h_{ch} = \pm 0.035$; uncertainty in U_τ, see Table 1; maximum random error in $\langle u'^2 \rangle^{1/2}$ and $\langle v'^2 \rangle^{1/2} = \pm 0.040$ and ± 0.010 m/s, respectively).

seem to be dependent on the blockage ratio, at least in the case of high values of this parameter. To confirm this last trend, future experiments involving higher blockage ratii are required.

2) For reacting wakes, a better rescaling is obtained in regions 1 and 2. This can be related to the insensitivity of the length of this region to a change of the obstacle shape. In the far wake, the gas expansion associated with the heat released by the combustion process induces a positive slope in the streamwise evolution of the longitudinal component of the mean velocity. This slope is obviously dependent on the rate at which the heat is released. Accordingly, in a region of intense heat release such as region 3, the equivalence ratio effects cannot by rescaled by the present and rather simple choice of reference values.

The same conclusions can be drawn when the more refined scaling proposed by Sullerey et al.[24] is used. Thus, it appears that as far as the similarity properties of the investigated wakes are concerned, no simple scaling is able to provide a unified representation of the flow involving the influence of the obstacle shape for inert wakes and the effect of the equivalence ratio for reactive wakes. As suggested by one of the reviewers, a better collapse for the reacting wakes might be obtained by using the gas density and velocity because the major effect of combustion is to change the gas density. This interesting suggestion has not been tested in the present study mainly based on velocity measurements.

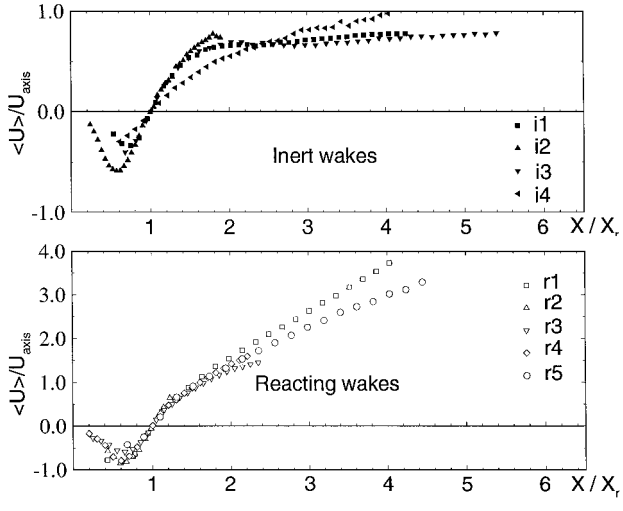

Fig. 5 Centerline evolution of the normalized mean streamwise velocity component in the wake of the flame holder (systematic error in x = ± 0.5 mm; uncertainty in X_r and U_{axis}, see Table 1; maximum uncertainty in $\langle U \rangle$ = ± 0.15 m/s).

Reynolds Stresses Profiles

The rms values of the longitudinal and transverse components of the velocity fluctuations normalized by U_{axis} are plotted as a function of the normalized abscissa x/X_r in Fig. 7. The transverse evolution of these quantities and the correlation between the two velocity components are shown in Fig. 8 against the normalized transverse coordinate. These figures show that for inert wakes the turbulence intensity and the shear stresses observed behind the rectangular section cylinder are twice as much as their counterparts behind the triangular section cylinder. This is no longer the case when combustion develops in the wake because no significant differences are observed for the wakes behind obstacles of different shapes. In such cases, the influence of combustion overcomes the influence of the obstacle shape.

Figure 8 shows also that for all the reactive wakes the intensity of the normal velocity fluctuations is smaller than its counterpart observed in the absence of combustion. As will be shown in the next section, this decrease could be the consequence of a restructuring of the large-scale unsteady part of the wake associated with the absence of vortex shedding in the reactive wakes. On the contrary, the intensity of the fluctuations of the streamwise velocity component

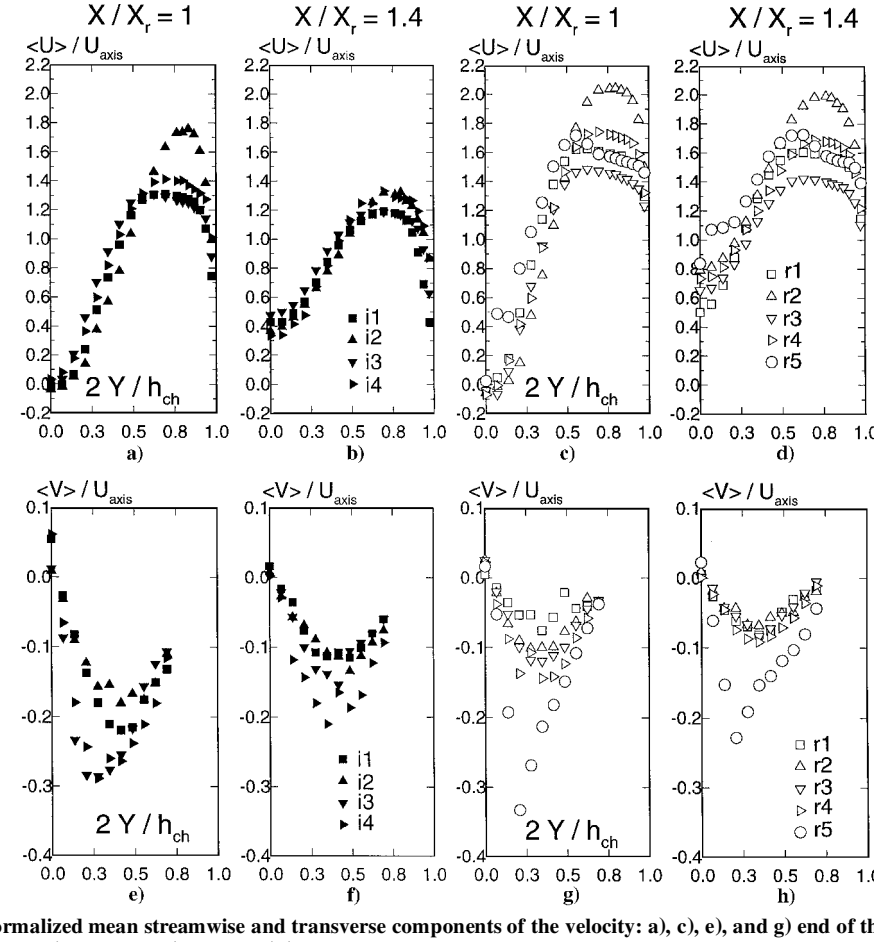

Fig. 6 Profiles of the normalized mean streamwise and transverse components of the velocity: a), c), e), and g) end of the mean recirculation zone (x/X_r = 1); and b), d), f), and h) near wake (x/X_r = 1.4) (systematic error in $2y/h_{ch}$ = ± 0.035; systematic error in x = ± 0.5 mm; uncertainty in X_r and U_{axis}, see Table 1; maximum uncertainty in $\langle U \rangle$ and $\langle V \rangle$ = ± 0.15 and ± 0.25 m/s, respectively).

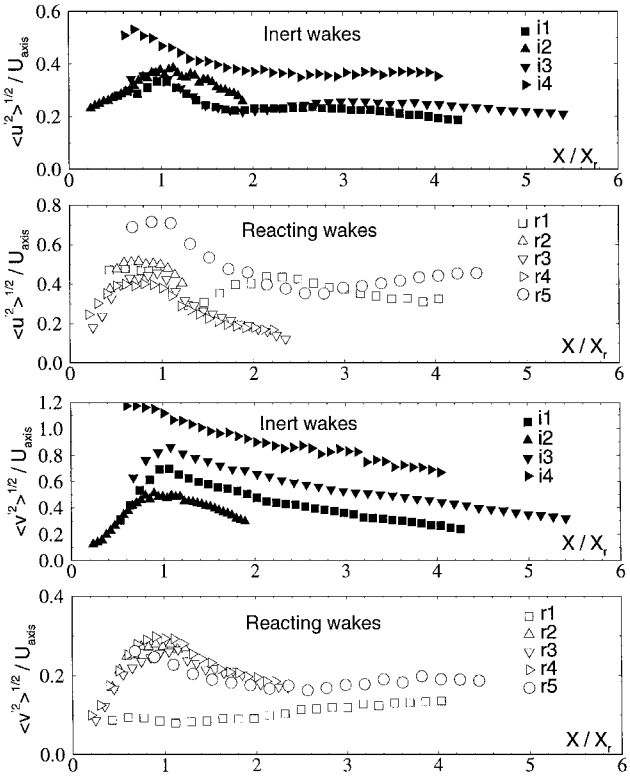

Fig. 7 Centerline evolution of the normalized rms longitudinal and normal velocity fluctuations in the wake of the flame holder (systematic error in $x = \pm 0.5$ mm; uncertainty in X_r and U_{axis}, see Table 1; maximum uncertainty in $\langle u'^2\rangle^{1/2}$ and $\langle v'^2\rangle^{1/2} = \pm 1.20$ and ± 2.10 m/s, respectively).

remains almost unchanged between inert and reactive wakes, except in case r5 for which larger values are observed when compared with case i3. As will be shown in the next section, this increase goes with the presence of a marked frequency on the associated spectra, thus indicating the existence of a pulsation of the wake in the streamwise direction. The fact that this effect is not observed in case r3 similar to case r1, except for the much smaller value of Re_{ch} in the latter case, indicates that this pulsation is directly related to a Reynolds number variation effect at constant ϕ.

Spectra and Histograms

As shown in the preceding section, the mean structure of the reactive wakes is qualitatively similar to that of the inert wakes because only local quantitative changes are observed. This is no longer the case as soon as the statistical and spectral properties are concerned. To illustrate this, the unsteady characteristics of wakes r3, r4, and r5 that feature all the main phenomena of the five reacting wakes studied here are compared with those of inert wakes i3 and i4, considered as the reference inert wakes. For all of these cases, the relative Reynolds number variation is less than 10%. In return, two largely different values of ϕ are considered ($\phi = 0.65$, cases r3 and r4, and $\phi = 0.85$, case r5) as well as two different obstacle shapes (rectangular section, cases i4 and r4, and triangular section, cases i3, r3, and r5). Figures 9 and 10 display the spectra and the associated PDFs of the two velocity components.

For the inert wakes i3 and i4, a distinct peak of energy is observed on the v' spectra for a frequency value of 220 ± 5 Hz (cases i3) and of 170 ± 5 Hz (case i4). This is a clear signature of the vortex shedding known to occur in such wakes as is the bimodal shape of the associated V PDFs.

The corresponding Strouhal number Sr based on h_{obs} and U_{axis} is found to be $Sr = 0.26 \pm 0.1$ and 0.21 ± 0.1 for cases i3 and i4, respectively. For cases i3, this is in close agreement with the experimental value of 0.23 reported by Fureby and Möller.[13] The level of

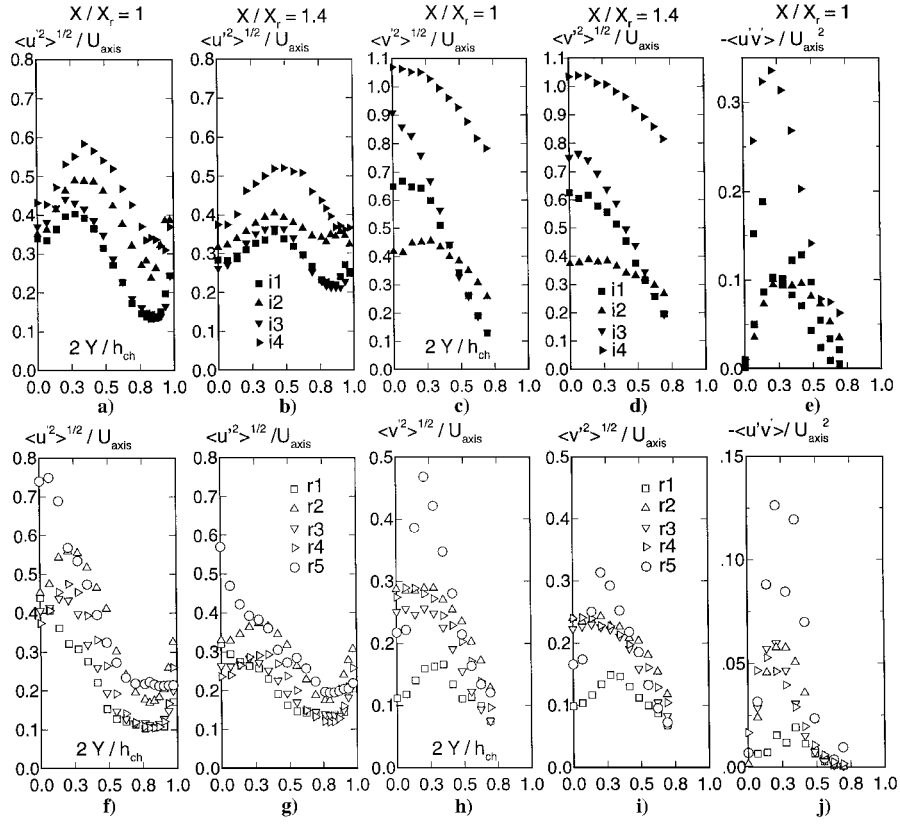

Fig. 8 Profiles of the rms longitudinal and normal velocity fluctuations and cross correlation: a), c), e), f), h), and j) end of the mean recirculation zone ($x/X_r = 1$); b), d), g), and i) near wake ($x/X_r = 1.4$) (systematic error in $2y/h_{ch} = \pm 0.035$; uncertainty in X_r and U_{axis}, see Table 1; maximum uncertainty in $\langle u'^2\rangle^{1/2}$, $\langle v'^2\rangle^{1/2}$, and $\langle u'v'\rangle = 1.10$ m/s, 1.90 m/s, and 1.30 m^2/s^2, respectively).

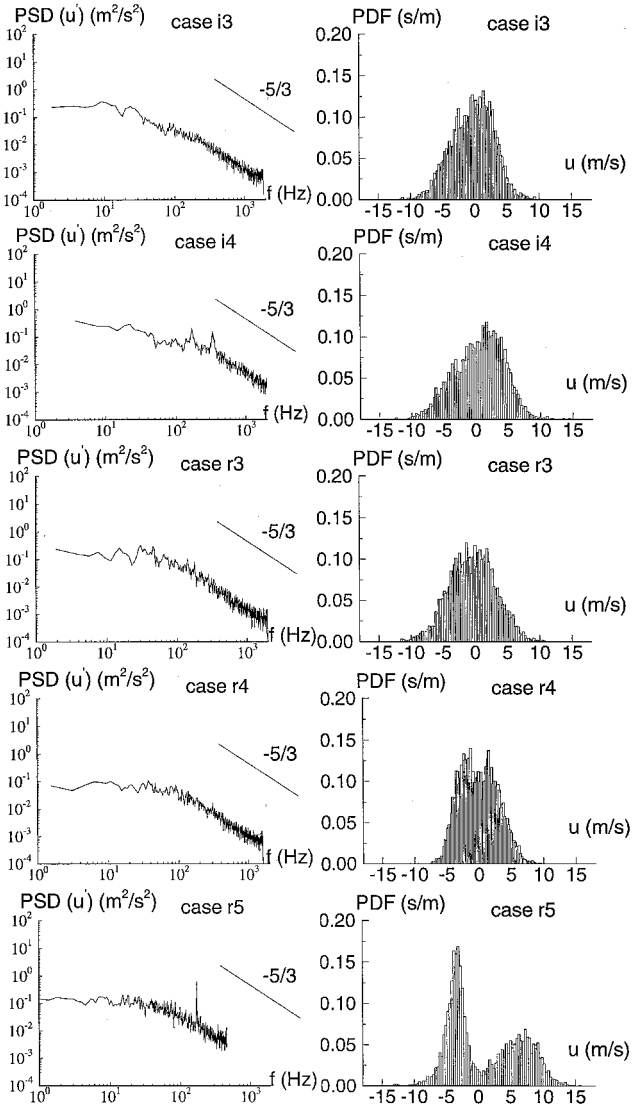

Fig. 9 Spectra and PDFs of the streamwise velocity fluctuations at the end of the recirculation zone ($x/X_r = 1$) (frequency and velocity resolutions = ± 2.5 Hz and ± 0.25 m/s, respectively; maximum relative uncertainty in PSD and PDFs = ± 5 and ± 5%, respectively).

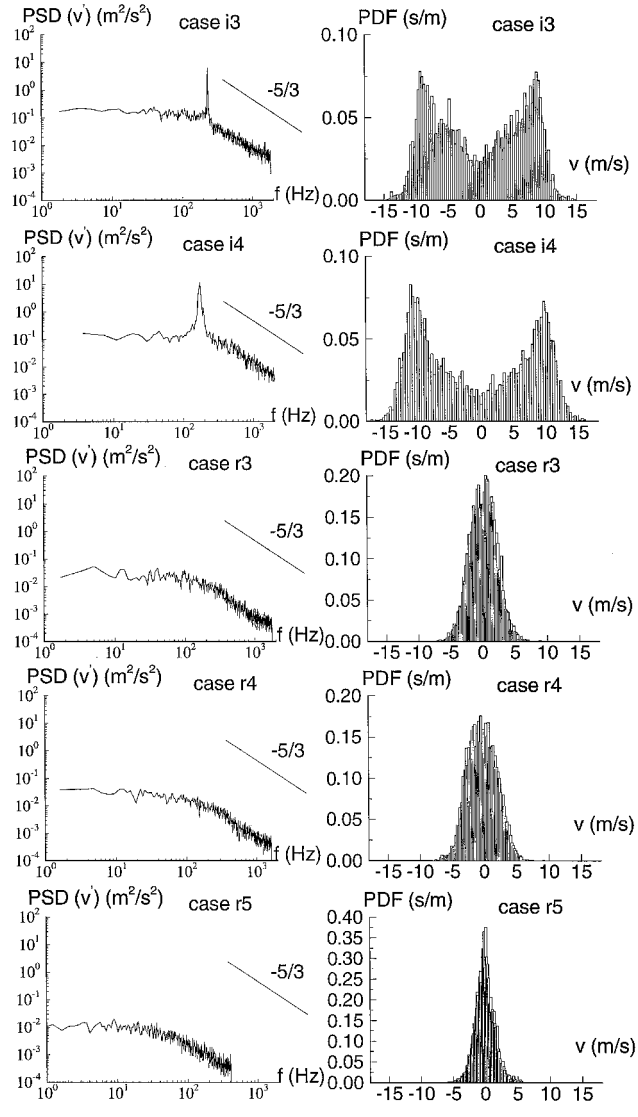

Fig. 10 Spectra and PDFs of the normal velocity fluctuations at the end of the recirculation zone ($x/X_r = 1$) (frequency and velocity resolutions = ± 2.5 Hz and ± 0.25 m/s, respectively; maximum relative uncertainty in PSD and PDFs = ± 4 and ± 5%, respectively).

the peak of energy is larger in case i4 than it is in case i3 in accordance with the higher intensity level measured for v'^2 in the former case.

For the reactive wakes, the picture is totally different. First, no peak of energy is observed on the v' spectra and the related PDFs exhibit a Gaussian-like behavior. Second, no noticeable sensitivity to the obstacle shape is observed. Consequently, these reactive wakes are only sensitive to Reynolds numbers or equivalence ratio variations. Thus, an important finding is the fact that the vortex shedding present in the inert wakes is no longer present in the reactive wakes. Such an absence goes with an important decrease of the level of the intensity of the normal velocity fluctuations that consequently cannot be attributed to the sole decrease of the turbulence intensity but has to be related to a dramatic change of the nature of the wakes.

Now, the question that comes along immediately is the following: does the absence of vortex shedding in the reactive wakes mean that no large-scale coherent structures exist in these wakes? On the one hand, the analysis of the spectra and PDFs of the longitudinal component of the velocity and, on the other, the characteristics of the temperature spectra in cases r3 and r5 (Fig. 11) strongly suggest that the answer to that question is no. Indeed, it appears that first a noticeable peak of energy around the frequency of 170 ± 5 Hz is present in the temperature spectrum for case r5. The fact that the same distinct peak of energy located around the same value of the frequency is observed also on the uncompensated temperature spectrum clearly indicates that this peak is a feature of the flow and is not caused by an overcompensation of the signal. In this latter case only, the u' spectra exhibits a distinct peak of energy around the same frequency value as the one observed for the temperature spectrum. In addition, a bimodal shape for the U PDF is obtained. The explanation for such a behavior is the existence of a symmetric flapping of the two flame fronts anchored at the edges of the obstacles, which is also visible on visualizations (not presented here) of the reactive wakes. Such a flapping is the cause of the longitudinal flow pulsation, which in case r3 is not sufficiently vigorous to have a distinguishable signature on the u' and T' spectra, whereas the larger equivalence ratio of case r5 makes this pulsation energetic enough to induce a clear signature on the both the u' and the T' spectra. Such a pulsation is also the cause of the modification of the inlet velocity profiles observed previously for case r5.

Consequently, if there is definitely a change of the large-scale structure nature of the reactive wakes, Figs. 9 and 10 show that the corresponding redistribution of the kinetic energy does not affect the spectra associated with the stochastic turbulence of the flow, which is always following a classical behavior, namely a $-5/3$ power law decay in its inertial range. A systematic comparison between the v' spectra of the inert and reactive wakes indicates that the overall energy contained in the scales corresponding to this inertial range is lower for the reactive wakes. This behavior is not observed on the u' spectra. More precisely, in presence of combustion the energy level of the decaying part of the energy spectra of v' becomes of the same

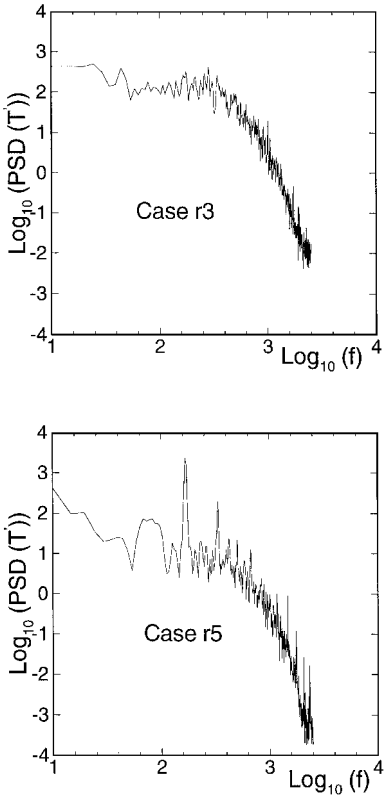

Fig. 11 Examples of temperature spectra in the near wake for cases r3 and r5 (x/X_r = 1.5 and $2y/h_{ch}$ = 0.6; frequency resolution = ± 2.5 Hz; maximum relative uncertainty in PSD = ± 3.5%).

order of magnitude as the one observed for the u' spectra except in case r5. Such a better equidistribution of the energy in the inertial range of the stochastic turbulence between the transverse and the streamwise motion is solely due to the decrease of the energy level of the whole spectra of v' in the presence of combustion, whereas the energy level of the spectra of u' is almost conserved between inert and reactive flows.

V. Concluding Remarks

We have given experimental results showing the sensitivity of the structure of the wakes behind bluff bodies to 1) the presence of exothermic chemical reactions, 2) the flow configuration and the Reynolds number, 3) the mixture composition, and 4) the shape of the flame holder. In spite of the analogy that exists between the mean structures of the wakes, no satisfactory classical similarity variables have been found to rescale in a unique way both the sensitivity of the inert wakes to the obstacle shape and the sensitivity of the reactive wakes to the equivalence ratio value. Nevertheless, a fair rescaling is obtained when these two effects are disregarded. The structure of the instantaneous wake was found to be dramatically different between inert and reactive wakes, thus indicating a total change of the large scales' unsteady motion. Indeed, whereas the signature of the vortex sheeding in the inert case consists of a marked frequency on the spectra associated with the transverse velocity component, the results obtained in the reactive wakes show that 1) there exist cases where no marked frequency at all is obtained on the velocity components, and 2) when a marked frequency is obtained for the velocity spectrum, this is for the streamwise component only and the same energetic frequency band is observed on the temperature signal spectrum. Thus such a sensitivity of the instantaneous properties of the reacting wakes to the equivalence ratio and the Reynolds number represents a great challenge as far as the development of large-eddy simulation of turbulent premixed flames is concerned. The present experimental results give as one of the objectives for such a type of simulation the test of its capability of reproducing the sensitivity of the instantaneous velocity field of bluff-body stabilized reacting wakes to the incoming flow properties.

References

[1]Calvert, J. R., "Experiments on Low-Speed Flow Past Cones," *Journal of Fluid Mechanics*, Vol. 27, No. 2, 1967, pp. 273–289.

[2]Brown, L. W. B., Antonia, R. A., and Bisset, D. K., "Coherent Structures in the Far Field of a Turbulent Wake," *Physics of Fluids*, Vol. 29, No. 11, 1986, pp. 3612–3617.

[3]Antonia, R. A., "Organization in a Turbulent Near-Wake," *Fluid Dynamics Research*, Vol. 7, 1991, pp. 139–149.

[4]Franke, R., and Rodi, W., "Calculations of Vortex Shedding Past a Square Cylinder with Various Turbulence Models," *Proceedings of 8th Symposium on Turbulent Shear Flows*, 1991, 20-1.

[5]Hosokawa, S., Ikeda, Y., and Nakajima, T., "Effect of Flame Holder Shape on Vortex Shedding," AIAA Paper 96-3130, July 1996.

[6]Williams, G. C., Hottel, H. C., and Scurlock, A. C., "Flame Stabilization and Propagation in High Velocity Gas Streams," *Third Symposium on Combustion, Flame and Explosion Phenomena*, Williams and Wilkins, Baltimore, MD, 1949, pp. 21–40.

[7]Heitor, M. V., Taylor, A. M. K. P., and Whitelaw, J. H., "Velocity and Scalar Characteristics of the Turbulent Premixed Flames Stabilized on Confined Axisymmetric Baffles," *Combustion Science and Technology*, Vol. 62, Nos. 1–3, 1988, pp. 97–126.

[8]Ballal, D. R., Chen, T. H., and Schmoll, W. J., "Fluid Dynamics of a Conical Flame Stabilizer," *Journal of Engineering for Gas Turbines and Power*, Vol. 111, Jan. 1989, pp. 97–102.

[9]Pan, J. C., Schmoll, W. J., and Ballal, D. R., "Turbulent Combustion Properties Behind a Confined Stabilizer," *Journal of Engineering for Gas Turbines and Power*, Vol. 114, Jan. 1992, pp. 33–37.

[10]Fujii, S., and Eguchi, K., "A Comparison of Cold and Reacting Flows Around a Bluff-Body Flame Stabilizer," *Transactions of the American Society of Mechanical Engineers*, Vol. 103, June 1981, pp. 328–334.

[11]Ferziger, J. H., and Leslie, D. C., "Large Eddy Simulation—A Predictive Approach to Turbulent Flow Computation," AIAA Paper 79-1441, July 1979.

[12]Fureby, C., and Löfström, C., "Large-Eddy Simulation of Bluff Body Stabilized Flames," *25th Symposium (International) on Combustion*, Combustion Inst., Pittsburgh, PA, 1994, pp. 1257–1264.

[13]Fureby, C., and Möller, S. I., "Large Eddy Simulation of Reacting Flows Applied to Bluff Body Stabilized Flames," *AIAA Journal*, Vol. 33, No. 12, 1995, pp. 2339–2347.

[14]Olsson, M., and Fuchs, L., "Large Eddy Simulation of the Proximal Region of a Spatially Developing Circular Jet," *Physics of Fluids*, Vol. 8, No. 8, 1996, pp. 2125–2137.

[15]Lee, D. H., and Sung, H. J., "Assessment of Turbulent Spectral Bias in Laser Doppler Velocimeter," *Experiments in Fluids*, Vol. 16, No. 3–4, 1994, pp. 223–235.

[16]Edwards, R. V., and Jensen, A. S., "Particle Sampling Statistics in Laser Anemometers: Sample-and-Holds Systems and Saturable Systems," *Journal of Fluid Mechanics*, Vol. 133, Aug. 1983, pp. 397–411.

[17]Benedict, L. H., and Gould, R. D., "Towards Better Uncertainties Estimates for Turbulence Statistics," *Experiments in Fluids*, Vol. 22, No. 2, 1996, pp. 129–136.

[18]Collis, D. C., and Williams, M. J., "Two Dimensional Convection from Heated Wires at Low Reynolds Number," *Journal of Fluid Mechanics*, Vol. 6, Pt. 3, 1959, pp. 357–384.

[19]Moffat, R. J., "Designing Thermocouples for Response Rate," *Transactions of the American Society of Mechanical Engineers*, Vol. 80, 1958, pp. 257–262.

[20]Heitor, M. V., Taylor, A. M. K. P., and Whitelaw, J. H., "Simultaneous Velocity and Temperature Measurements in a Premixed Flame," *Experiments in Fluids*, Vol. 3, No. 6, 1985, pp. 323–339.

[21]Heitor, M. V., and Moreira, L. N., "Thermocouples and Samples Probes for Combustion Studies," *Progress in Energy and Combustion Science*, Vol. 19, No. 3, 1993, pp. 259–278.

[22]Comte-Bellot, G., "Écoulements Turbulents entre Deux Plaques Parallèles," Ph.D. Thesis, Université de Grenoble, Grenoble, France, 1963.

[23]Eckelmann, H., "The Structure of the Viscous Sublayer and the Adjacent Wall Region in a Turbulent Channel," *Journal of Fluid Mechanics*, Vol. 65, No. 3, 1974, pp. 439–459.

[24]Sullerey, R. H., Gupta, A. K., and Moorthy, C. S., "Similarity in the Turbulent Near Wake of Bluff Bodies," *AIAA Journal*, Vol. 13, No. 11, 1975, pp. 1425–1429.

W. Oberkampf
Associate Editor